*electronics*

MDPI

*Article*

# A Study on the Detecting Cycle Slips and a Repair Algorithm for B1/B3

**Yanchen Dong [1,†], Peipei Dai [1,†], Sen Wang [1], Jianping Xing [1,*], Yulei Xue [2], Shijie Liu [1], Shuai Han [1], Zhi Yang [1] and Xinchao Bai [1]**

[1] School of Microelectronics, Shandong University, Jinan 250100, China; 201942267@mail.sdu.edu.cn (Y.D.); 202020312@mail.sdu.edu.cn (P.D.); 202120349@mail.sdu.edu.cn (S.W.); 202032465@mail.sdu.edu.cn (S.L.); 201932243@mail.sdu.edu.cn (S.H.); 201932264@mail.sdu.edu.cn (Z.Y.); 201942265@mail.sdu.edu.cn (X.B.)
[2] School of Information Science and Engineering, Shandong University, Qingdao 266237, China; 201820310@mail.sdu.edu.cn
* Correspondence: xingjp@sdu.edu.cn
† These authors contributed equally to this work.

**Abstract:** For the current problem of cycle slips in the observation data of the BDS-2 and BDS-3 (Bei Dou Navigation Satellite System), in this paper, BDS B1I and B3I signals are used as research objects to study the detection of cycle slips, and their repair algorithm. The Geometry-free (GF) and Melbourne–Wübeena (MW) combination algorithm are used for the detection of cycle slips. A new method of arc partition is proposed in this work to detect cycle slips as the boundary to delimit two different observation arcs. In this way, the different values of cycle slips can be divided and marked. Moreover, the gross errors can be removed. Finally, the detection of cycle slips and the analysis of all epochs can be completed and repaired. This work also analyzes the dual-frequency data effect of cycle slips on code multipath observation. The results showed that this method greatly improved the speed of detection of cycle slips.

**Keywords:** BDS; cycle slips; geometry-free combination; Melbourne–Wübeena combination; turbo edit method; code multipath; arc partition



**Citation:** Dong, Y.; Dai, P.; Wang, S.; Xing, J.; Xue, Y.; Liu, S.; Han, S.; Yang, Z.; Bai, X. A Study on the Detecting Cycle Slips and a Repair Algorithm for B1/B3. *Electronics* **2021**, *10*, 2925. https://doi.org/10.3390/electronics10232925

Academic Editor: Manuel Arrebola

Received: 21 October 2021
Accepted: 23 November 2021
Published: 25 November 2021



## 1. Introduction

With the development of the Global Navigation Satellite System (GNSS), and with the BDS-3 constellation having successfully been fully networked, users have higher and higher requirements for high-precision and real-time positioning [1–3]. In precision positioning, the accuracy of carrier phase positioning (centimeter-level) is higher than pseudo-range positioning (meter level) [4,5]. In practice, the building occlusion, ionospheric changes, and receiver hardware delay [6] cause the cycle counter of the receiver to jump, which causes cycle slips and seriously affects positioning accuracy. Currently, the conventional methods of cycle slip processing include the high-order differentials, Doppler integration, the Melbourne–Wübeena (MW) combination, Geometry-free (GF) combination and the TurboEdit method [6,7]. The high-order difference is a relatively simple method for detecting cycle slips. If the difference is more than three times between adjacent epochs, it is the high-order difference. Although the high-order difference can be used to weaken the receiver clock bias, satellite clock bias, ionospheric delay and troposphere delay, as the order of difference increases, cycle slips and the accumulation of residual errors will occur [8]. This method can detect large value cycle slips, but it is difficult to detect cycle slips with less than five cycles. However, the accuracy of the Doppler integration method to detect cycle slips depends on the Doppler observations. Meanwhile, due to the different accuracy of Doppler observations obtained by different receivers, it was difficult to use this method on low-precision receivers. Moreover, the MW combination method has real-time functionality, but it cannot detect equivalent cycle slip combinations [9,10].

Furthermore, the GF method uses ionospheric residuals to detect cycle slips, but there is the multi-value problem, and it is also difficult to detect specific cycle slips. In addition, TurboEdit combines MW and GF through dual-frequency carrier phase [4] and pseudo-range observations with higher reliability. The rest of the paper is structured as follows. Section 2 presents the cycle slip detection method that contains the MW combination method, the GF combination method, the TurboEdit method and the code multipath observation method. Sections 3 and 4 introduce the experimental design and results. In this contribution, we use this method to detect and repair cycle slips of BDS B1I and B3I signals. Furthermore, we propose a new arc partition method to improve the efficiency of the detection of cycle slips. Section 5 presents an experimental analysis of the new arc partition method. Section 6 introduces the conclusions of this paper and the prospects of future work.

## 2. Cycle Slips Detection Methods

### *2.1. MW Combination Method*

The MW combination method uses the wide lane value of the carrier phase to subtract the narrow lane value of the pseudorange, then combine them together. This method can weaken the influence of the ionosphere and troposphere and obtain the combined observation value of MW [11,12]. The MW combination observations equation [13] can be expressed as:

$$L_{mw} = \frac{1}{f_1 - f_3}(f_1 L_1 - f_3 L_3) - \frac{1}{f_1 + f_3}(f_1 P_1 + f_3 P_3) \quad (1)$$

where $L_{mw}$ represents the MW combination observations; $f_1$ denotes the carrier frequency of the B1I signal; $f_3$ denotes the carrier frequency of the B3I signal; $P_1$ refers to the pseudo-range observations of the B1I signal; $P_3$ refers to the pseudo-range observations of the B3I signal; $L_1$ indicates the carrier observations of the B1I signal; and $L_3$ indicates the carrier phase of the B3I signal.

Through the above equation, the ambiguity of the combined observation value can be described as:

$$N_{mw} = \frac{L_{mw}}{\lambda_{mw}} \quad (2)$$

and

$$\lambda_{mw} = \frac{c}{f_1 + f_3} \quad (3)$$

where $N_{mw}$ indicates the combined ambiguity of the MW; $\lambda_{mw}$ represents the combined wavelength of MW combination, $c$ is the speed of light.

The MW combination method can eliminate the receiver clock bias, satellite clock bias [14] and ionospheric delay by finding the mean value of $N_{mw}$, denoted by $\overline{N_{mw}}$. Then, the difference is compared with the variance of this epoch if the value of $\left|N_{mw}(i) - \overline{N}_{mw}(i-1)\right|$ is four times greater than the variance. Simultaneously, when the value of $|N_{mw}(i) - N_{mw}(i+1)|$ is less than 1, it is determined that the generation cycle slips. The corresponding formula can be expressed as:

$$\left|N_{mw}(i) - \overline{N}_{mw}(i-1)\right| \geq 4\sigma(i-1) \quad (4)$$

and

$$|N_{mw}(i) - N_{mw}(i+1)| \leq 1 \quad (5)$$

where $N_{mw}(i)$ is the $i$-th epoch ambiguity; $\overline{N}_{mw}(i)$ represents the $i$-th epoch average ambiguity; $\sigma(i)$ indicates the variance in the $i$-th epoch MW combination observations.

Where in, the $\overline{N}_{mw}(i)$ and $\sigma(i)$ can be described as:

$$\backslash \overline{N}_{mw}(i) = \overline{N}_{mw}(i-1) + \frac{1}{i}\left[N_{mw}(i) - \overline{N}_{mw}(i-1)\right] \tag{6}$$

and

$$\backslash \sigma^2(i) = \sigma^2(i-1) + \frac{1}{i}[\left(N_{mw}(i) - \overline{N}_{mw}(i-1))^2 - \sigma^2(i-1)\right] \tag{7}$$

### 2.2. GF Combination Method

The GF combination method performs cycle slip [15] detection by combining carrier phase observations and pseudo-range observations; $L_{GF}$ can be described as:

$$L_{GF} = L_1 - L_3 + P_1 - P_3 \tag{8}$$

where $L_{GF}$ is the carrier phase observations.

Since the accuracy of the ionospheric delay difference $P_1 - P_3$ is lower than the carrier phase [16], $L_{GF}$ is generally subjected to a further polynomial fit obtained by fitting $Q_{GF}$, the fitting order is $m = \min(\mathrm{n}/100 + 1.6)$, and $n$ is the total epoch number [17].

Then, the cycle slips are detected as:

$$|[L_{GF}(i) - Q_{GF}(i)] - [L_{GF}(i-1) - Q_{GF}(i-1)]| > 6(\lambda_3 - \lambda_1) \tag{9}$$

and

$$\backslash |[L_{GF}(i) - Q_{GF}(i)] - [L_{GF}(i+1) - Q_{GF}(i+1)]| < (\lambda_3 - \lambda_1) \tag{10}$$

where $\lambda_1$ denotes the wave length of the B1I signal; $\lambda_3$ denotes the wave length of the B3I signal.

When the conditions of $|[L_{GF}(i) - Q_{GF}(i)] - [L_{GF}(i-1) - Q_{GF}(i-1)]|$ being six times greater than $\lambda_3 - \lambda_1$ and $|[L_{GF}(i) - Q_{GF}(i)] - [L_{GF}(i+1) - Q_{GF}(i+1)]|$ being less than $\lambda_3 - \lambda_1$ are satisfied at the same time, the epoch of a cycle slip is thought to occur.

When the $L_1$ and $L_3$ difference is less than seven cycles, GF combination method can detect cycle slips [18]. However, when the cycle slips are too large, they are difficult to detect accurately.

### 2.3. TurboEdit Method

The TurboEdit method combines the MW and GF methods for cycle slip detection [19]; it can be then written as:

$$L_{mw} = \lambda_{mw}(N_1 - N_3) \tag{11}$$

and

$$\backslash L_{GF} = \lambda_1 N_1 - \lambda_3 N_3 - Q_{GF} \tag{12}$$

where $N_1$ indicates the ambiguity of the B1I signal and $N_3$ indicates the ambiguity of the B3I signal;

The values of $N_1$ and $N_3$ can be obtained by solving the system of equations. When $N_1 - N_3 = 0$, the MW combination method fails. When $N_1 = (f_1/f_3)N_3$, the GF combination method fails. By using the TurboEdit method for combination, we can effectively avoid the shortcomings of the MW combination and the GF combination method. The advantages are obvious, namely that the TurboEdit method can improve the accuracy of the detection of cycle slips. However, the TurboEdit method is affected by the ionospheric delay and the sampling rate [20]. Therefore, the higher the sampling rate is, the smaller ionospheric delay is, but when the sampling rate is increased, the amount of data becomes larger, and the data is processed with higher efficiency. It is necessary to further explore how to quickly find the cycle slip values in the entire observation arc.

### *2.4. Code Multipath Observation*

By combining and comparing the B1/B3 dual-frequency code multipath [21] before and after repairing, it is established that the formulas are as follows [22,23]:

$$M_1 = P_1 - L_1 + 2{\lambda_1}^2 \frac{L_3 - L_1}{{\lambda_3}^2 - {\lambda_1}^2} \tag{13}$$

and

$$\backslash M_3 = P_3 - L_3 + 2{\lambda_3}^2 \frac{L_1 - L_3}{{\lambda_1}^2 - {\lambda_3}^2} \tag{14}$$

where $M_1$ is the code multipath value of the B1I signal; $M_3$ is the code multipath value of the B3I signal.

## 3. Experimental Design

In this study, the Perth station provided by iGMAS was selected for this experiment. The data covered day of year (DOY) 108, 2018. The observation time was chosen to be the DOY 108, 2018. The TurboEdit method was mainly used for cycle slip detection, and a new arc partition method based on RMS (Root Mean Square) was adopted to divide the entire observation arc to the improve the efficiency of cycle slip detection.

$$RMS = \sqrt{(X_1 - (X_1 + \cdots + X_n)/n)^2 + \cdots + (X_n - (X_1 + \cdots + X_n)/n)^2} \tag{15}$$

where $X_1$ to $X_n$ refer to the 1st to nth samples.

Firstly, according to the epoch cycle, the combined values of MW and GF of each satellite, where MW and GF combined values were mainly used for cycle slip detection, were calculated. Secondly, if the RMS of all MW combined observation values in an arc was greater than 0.5, it was considered that the cycle slips occurred in this observation arc. For Figure 1, the process for the detection of cycle slips was as follows:

1. The observation arc was divided into two sub-arcs of equal length. The sub-arc with larger RMS containing the cycle slips was called sub-arc 1, and the other arc, which did not contain cycle slips or contained a smaller cycle slip, was called sub-arc 2;
2. Starting from the end close to sub-arc 2, all epochs in sub-arc 1 were traversed. If the difference between the value of a certain epoch and the mean value of sub-arc 2 was greater than the MW combined cycle slip determination threshold of 3.5, the cycle slip was considered to have occurred at this epoch.
3. The epoch of the cycle slip was taken to be the dividing point, and the observation arc was divided into two new sub-arcs. If the RMS of the new sub-arc was greater than the threshold of 0.5, then the gross error was marked with a median error greater than three times the standard value. It was possible that the RMS of the arc was exceeded due to a cycle slip that had not yet been detected.
4. If both values of the arcs exceeded the limit by more than 3.5, the cycle slip of the first segment was calculated first, and the entire observation arc was repaired. Otherwise, the cycle slip was calculated according to the current arc, was corrected for the entire observation arc, and two new sub-arcs were connected. The set gross error mark was removed, the RMS of the entire continuous observation arc was recalculated, and the next cycle slip was detected until all cycle slips were detected and repaired.
5. Finally, as the criterion to eliminate gross errors for the entire observation arc, the median error was taken to be greater than 3 or 4 times.

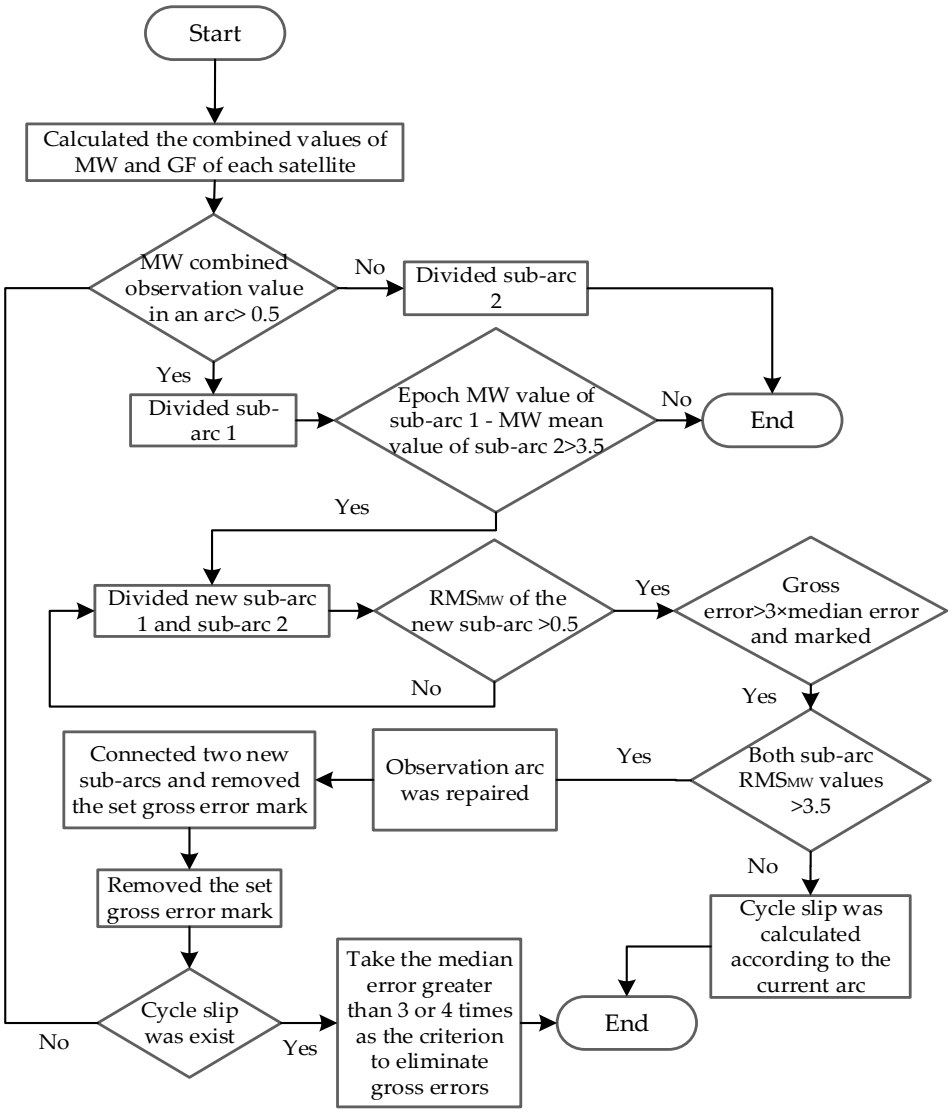


**Figure 1.** Flow chart of new arc partition method.

## 4. Experimental Results

In the experiment, three different orbit types of satellites were selected, namely the Geostationary Earth Orbit (GEO) satellite PRN 4, the Geosynchronous Orbit (IGSO) satellite PRN 6 and the Medium Earth Orbit (MEO) satellite PRN 22. Among them, PRN 4 and PRN 6 were Beidou-2 satellites, and PRN 22 was a Beidou-3 satellite.

Figure 2a–c represent the GF combination value of satellites PRN 4, PRN 6 and PRN 22, respectively, before the cycle slips were repaired. Figure 3a–c show the MW combination values before the cycle slips were repaired.

Before the cycle slips were repaired, the GF and MW combination values of three satellites with different orbits were observed. The satellite PRN 4 produced a cycle slip at the 868th epoch, in which the GF combination value jumped for about 2.5 cycles and the MW combination value jumped for about 5.5 cycles. The PRN 6 satellite produced a value jump at the 868th epoch, in which the GF combination value jumped for about 3.8 cycles and the MW combination value jumped for about 13.8 cycles. The PRN 22 satellite produced a value jump at the 822th epoch, in which the GF combination value jumped for about 5.9 cycles and the MW combination value jumped for about 35.3 cycles. Thus, it was presumed that the satellites PRN 4, PRN 6 and PRN 22 produced circumferential jumps at the above epochs.

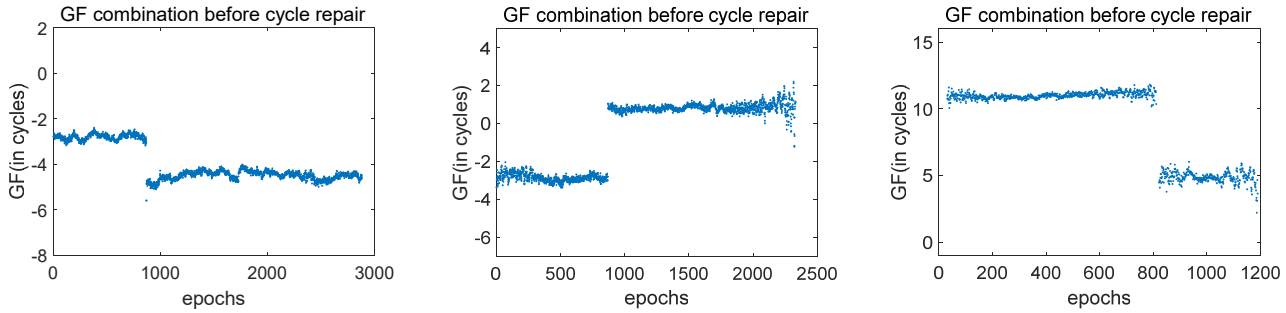


(**a**) (**b**) (**c**)

**Figure 2.** GF combination values before cycle slips were repaired.

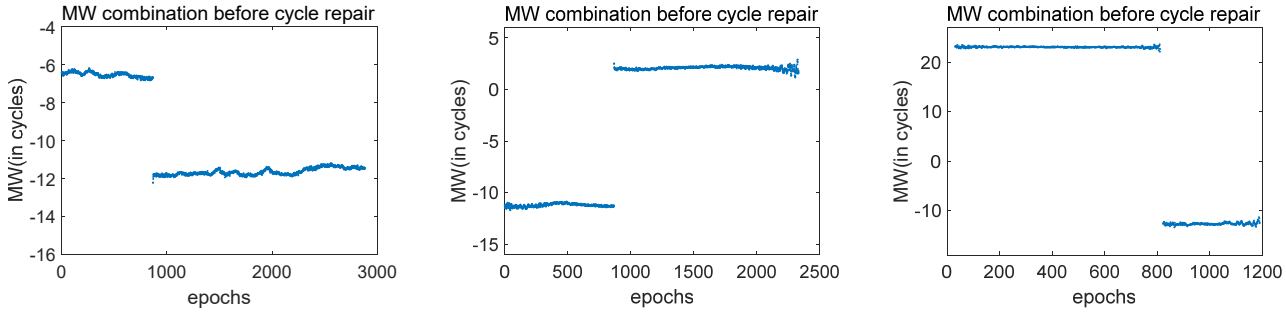


(**a**) (**b**) (**c**)

**Figure 3.** MW combination values before cycle slips were repaired.

Figure 4a–c represent the GF combination values of PRN 4, PRN 6 and PRN 22, respectively, after the cycle slips were repaired. Figure 5a–c show the MW combination values after the cycle slips were repaired. By comparing the experimental results obtained during the observation of PRN 4, we can conclude that, using TurboEdit method, a cycle slip was detected at the 868th epoch, and the corresponding solution denoted by $\Delta N_1$ was $-12$ cycles, and that denoted by $\Delta N_3$ was $-17$ cycles. Simultaneously, in combination with the results obtained for PRN 6, conclusions can be drawn from the detection of a cycle slip in the 868th epoch, using the TurboEdit method, for which the corresponding solution denoted by $\Delta N_1$ was 14 cycles and that of $\Delta N_3$ was 27 cycles. By comparing the experimental results of observation satellite PRN 22, we derived, using the TurboEdit method to detect the 822th epoch cycle slip, a corresponding $\Delta N_1$ solution of 48 cycles and an $\Delta N_3$ solution of 13 cycles.

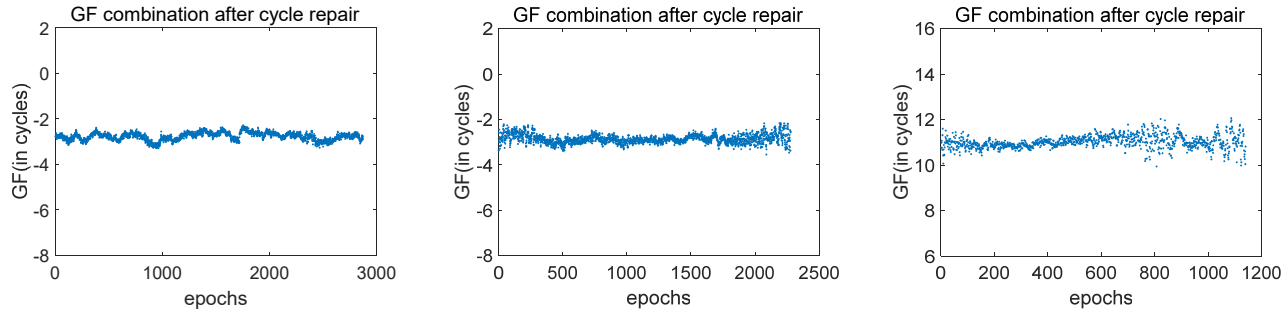


(**a**) (**b**) (**c**)

**Figure 4.** GF combination values after cycle slips were repaired.

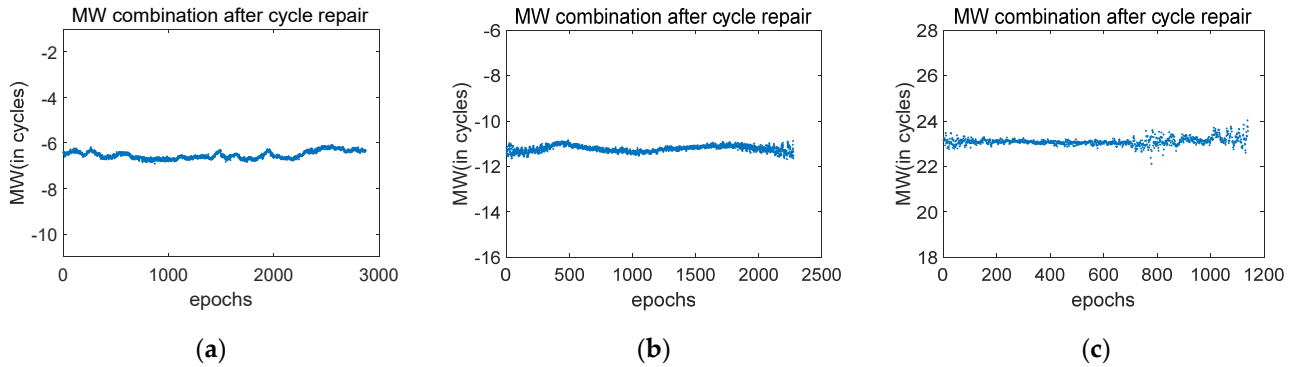


**Figure 5.** MW combination values after cycle slips were repaired.

In addition, Figure 6 shows the combined multipath values of the B1 and B3 frequencies before the cycle slips were repaired and Figure 7 shows the combined multipath values of the B1 and B3 frequencies after the slips were repaired. From the results shown in Table 1, we drew conclusions regarding the observation results of the combined multipath values of the B1 and B3 frequencies. When cycle slips were detected at the 868th epoch of PRN 4, a dual-frequency code multipath occurred with a 4.4029 m value jump at the B1I frequency and a 6.3651 m value jump at the B3I frequency. After the cycle slips were repaired, the Standard Deviation (STD) value of the dual-frequency code multipath was reduced from 0.5899 to 0.2210 at the B1I frequency and from 1.3903 to 0.2214 at the B3I frequency. When cycle slips were detected at the 868th epoch of PRN 6, a dual-frequency code multipath occurred with a 11.6586 m value jump at the B1I frequency and a 16.466 m value jump at the B3I frequency. After the cycle slips were repaired, the dual-frequency code multipath's STD value was reduced from 5.6354 to 0.1855 at the B1I frequency and from 7.4093 to 0.1366 at the B3I frequency. When cycle slips were detected at the 822th epoch of PRN 22, a dual-frequency code multipath occurred with a 32.7067 m value jump at the B1I frequency and a 38.5714 m value jump at the B3I frequency. After the cycle slips were repaired, the dual-frequency code multipath's STD value was reduced from 15.4003 to 0.2428 at the B1I frequency and from 18.2627 to 0.1721 at the B3I frequency.

It can be seen that after the cycle slips were repaired, the multipath value jumps were eliminated, and the detection of cycle slips could also be assisted by mutation of the multipath value. The code multipath value corresponding to the epoch that generated cycle slips also underwent a jump. After the cycle slips were repaired, the code multipath values of PRN 4, PRN 6 and PRN 22 was restored to values close to 0 m. It could be seen that the code multipath value of the dual frequency could also be used for the detection of cycle slips. Furthermore, we could also use the TurboEdit method in combination with the above approach to reduce the occurrence of the detection of cycle slips being missed.

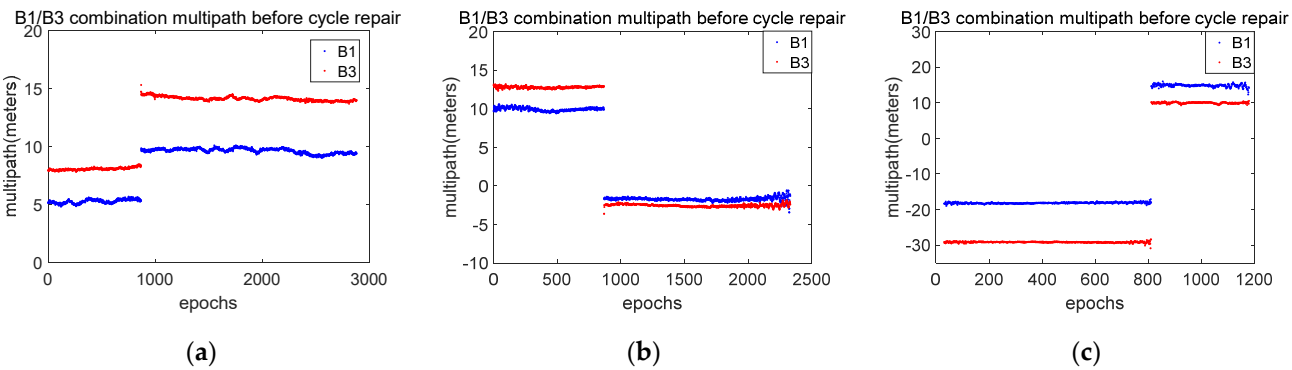


**Figure 6.** Combined multipath values for the B1 and B3 frequencies before the cycle slips were repaired.

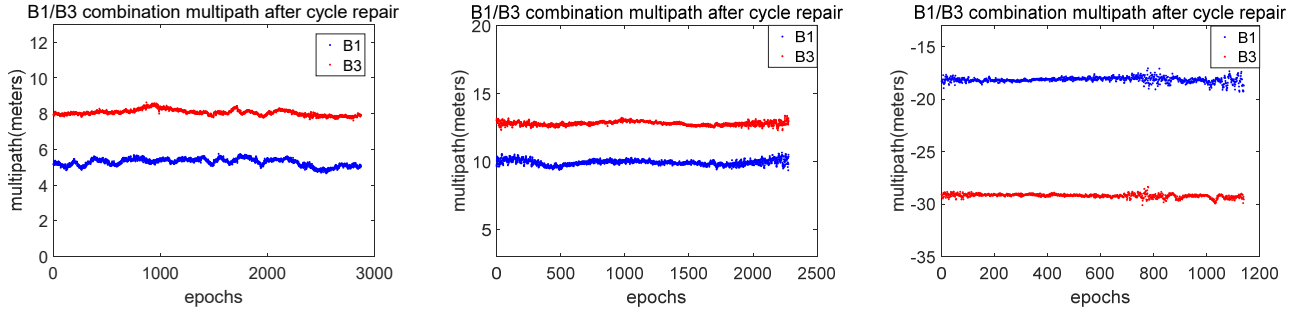


**Figure 7.** Combined multipath values of the B1 and B3 frequencies after the cycle slips were repaired.

**Table 1.** Observation results of combined multipath values of the B1 and B3 frequencies.

| PRN | Epoch | Value Jump (Meters) | | Code Multipath STD Value (Meters) before Cycle Slips Were Repaired | | Code Multipath STD Value (Meter) after Cycle Slips Were Repaired | |
|---|---|---|---|---|---|---|---|
| | | B1I | B3I | B1I | B3I | B1I | B3I |
| 4 | 868th | 4.4029 | 6.3651 | 2.0085 | 2.7807 | 0.2029 | 0.1607 |
| 6 | 868th | 11.6586 | 16.466 | 5.6354 | 7.4093 | 0.1855 | 0.1366 |
| 22 | 822th | 32.7067 | 38.5714 | 15.4003 | 18.2627 | 0.2428 | 0.1721 |

## 5. Experimental Analysis

By comparing and analyzing the above results, we can conclude that cycle slips can be detected and repaired by a new method of arc partition. Method 2 represents the new arc partition method. Method 1 represents the traditional sequential detection method of cycle slip analysis.

To further analyze the improvement of calculation efficiency, the improvement percentages of six group experiments are shown in Figure 8. As shown in Figure 8, compared with Method 1, the improvement range for Method 2 of PRN4 was 88.22 to 87.34%. Meanwhile, the improvement range of PRN6 was 67.88 to 69.71% and that of PRN22 was 25.76 to 30.19%. Furthermore, Table 2 expresses the STD values of the processing times for the selected satellites using two methods. The STD values of PRN4, PRN6 and PRN22 were less than 0.1. Therefore, it can be proven that the repeated test data have high stability and reliability. At the same time, the stability of Method 2 was found to be higher than that of Method 1, which implies more advantages in cycle slip detection with a large amount of data.

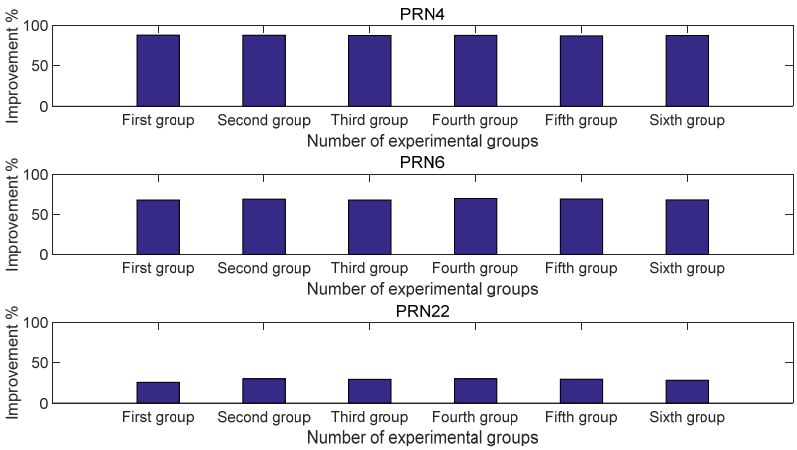


**Figure 8.** The running time of two methods for PRN 4, PRN 6 and PRN 22.

**Table 2.** STD values of the processing times of selected satellites using the two methods.

| PRN | 4 | 6 | 22 |
|---|---|---|---|
| STD value of Method 1 (s) | 0.0074 | 0.0102 | 0.0107 |
| STD value of Method 2 (s) | 0.0028 | 0.0021 | 0.0045 |

## 6. Conclusions

In this present work, we studied the detection of B1/B3 cycle slips and the algorithms used for their repair. Then, we analyzed the GF combination method, the MW combination method and the TurboEdit method, respectively. Finally, the TurboEdit method was adopted for the detection of cycle slips while using a new method of arc partition based on RMS size. In the experiment, we selected three satellites PRN 4, PRN 5 and PRN 22, with different orbits. PRN 4 and PRN 6 were Beidou-2 satellites and PRN 22 was a Beidou-3 satellite. The detection of cycle slips was performed by using a new method of arc partition combined with the TurboEdit method. The combined values of the GF and MW methods before and after the cycle slips were repaired, within the epochs of the three satellites, were analyzed, and the cycle slips were accurately detected. The TurboEdit method was adopted to perform the repair. After the repair was completed, the combined values of the GF and MW methods were compared with those before the repair to verify that cycle slips had been completed. Upon further observation of B1/B3 dual-frequency code multipath values, it was found that the code multipath also exhibited a value jump at the epoch where the cycle slips occurred. After the cycle slips were repaired, the code multipath value jump could be repaired to a value close to 0 m, and the TurboEdit method could be united for combined detection to reduce the occurrence of cycle slips and to further improve the accuracy of dual-frequency positioning. In the end, when comparing the running time of the new method of arc partition and the traditional cycle slip detection method of sequential detection, it was shown that the speed of detection of cycle slips was significantly increased in the experiments conducted in this study. At the same time, the cycle slips could be observed by using the code multipath value. In future work, the ionospheric residual method and the code multipath observation method will be combined with the TurboEdit method to improve the efficiency of the algorithm. In this way, the speed of detection of cycle slips will be further improved.

**Author Contributions:** Conceptualization, Y.D. and P.D.; methodology, Y.D., P.D. and S.W.; software, Y.D. and P.D.; validation, P.D. and S.H.; formal analysis, Y.D. and P.D.; investigation, X.B., S.L. and Y.X.; resources, J.X.; writing—original draft preparation, Y.D. and P.D.; writing—review and editing, Y.D., P.D., S.W. and Z.Y.; supervision, J.X. and P.D.; project administration, J.X.; All authors have read and agreed to the published version of the manuscript.

**Funding:** This research was funded by the Beidou New Time-space Intelligent Industry Development Collaborative Innovation Center (No. 0508-2).

**Informed Consent Statement:** Informed consent was obtained from all subjects involved in the study.

**Data Availability Statement:** The data used to support the findings of this study are available from the corresponding author upon request.

**Conflicts of Interest:** The authors declare that they have no conflict of interest.

## References

1. Zhen, D.; Knedlik, S.; Loffeld, O. Real-Time Cycle-Slip Detection and Determination for Multiple Frequency GNSS. In Proceedings of the Workshop on Positioning, Hannover, Germany, 2 May 2008.
2. Zumberge, J.F.; Heflin, M.B.; Jefferson, D.C.; Watkins, M.M.; Webb, F.H. Precisepoint Positioning for the Efficient and robust Analysis of GPS Data from Large Networks. *J. Geophys. Res.* **1997**, *102*, 5005–5017. [CrossRef]

3. Yuan, H.; Zhang, Z.; He, X.; Xu, T.; Zang, N. Real-time cycle slip detection and repair method for BDS-3 five-frequency data. *IEEE Access* **2021**, *99*, 1. [CrossRef]
4. Zhang, Y.C. Positioning of high earth orbit satellite using GPS/Beidou combined system. *Chin. J. Space Sci.* **2012**, *36*, 267–272.
5. Robustelli, U.; Baiocchi, V.; Pugliano, G. Assessment of Dual Frequency GNSS Observations from a Xiaomi Mi 8 Android Smartphone and Positioning Performance Analysis. *Electronics* **2019**, *8*, 91. [CrossRef]
6. Ke, J.; Lu, X.; Wang, X.; Chen, X.; Tang, S. Decoding Performance Analysis of GNSS Messages with Land Mobile Satellite Channel in Urban Environment. *Electronics* **2018**, *7*, 273. [CrossRef]
7. Yu, S.; Liu, Z. The ionospheric condition and GPS positioning performance during the 2013 tropical cyclone usagi event in the hong kong region. *Earth Planets Space* **2021**, *73*, 1–16. [CrossRef]
8. Sijie, L.; Xiang, Y.; Yu, W.; Wang, W. BDS-3 Triple Frequency Satellite Inter-frequency Clock Bias Estimation and Its Effects on Precise Point Positioning. In Proceedings of the China Satellite Navigation Conference (CSNC 2021), Nanchang, China, 26–28 May 2021.
9. Li, D.; Dang, Y.; Yuan, Y.; Mi, J. A New Cycle-Slip Repair Method for Dual-Frequency BDS Against the Disturbances of Severe Ionospheric Variations and Pseudoranges with Large Errors. *Remote Sens.* **2021**, *13*, 1037. [CrossRef]
10. Chen, X.H.; Tian, H.; Wang, T. Research on cycle slip detection and repair method of BDS/ GPS dual-difference combined data. *Sci. Surv. Mapp.* **2020**, *45*, 33–40.
11. Cai, C.; Liu, Z.; Xia, P.; Dai, W. Cycle slip detection and repair for undifferenced GPS observations under high ionospheric activity. *GPS Solut.* **2012**, *17*, 247–260. [CrossRef]
12. Zheng, Z.Y.; Cheng, Z.Y.; Huang, C.; Lu, X.S. Improving of Cycle Slip Detection and Correction of Blewitt Method. *Acta Astron. Sin.* **2005**, *46*, 216–224.
13. Gan, Y.; Sui, L.; Guo, B.Q.; Wen, J. Improving the performance of mw combined observation on cycle slip detection using emd threshold de-noising. *J. Geomat. Sci. Technol.* **2015**, *35*, 666–670.
14. Wang, G.; Jong, K.D.; Li, X.; Zhao, Q.; Guo, J. Analysis of characteristics of BDS observable combinations for wide-lane integer ambiguity resolution. In *China Satellite Navigation Conference (CSNC), 2014, Proceedings*; Springer: Berlin/Heidelberg, Germany, 2014; pp. 411–425.
15. Qian, N.; Gao, J.; Li, Z.; Li, F.; Pan, C. GPS/BDS triple-frequency cycle slip detection and repair algorithm based on adaptive detection threshold and FNN-derived ionospheric delay compensation. *Acta Geodyn. Geomater.* **2020**, *17*, 141–156. [CrossRef]
16. Zhang, S.; Yao, Y. Research on Cycle Slip Detection Methods for Un-difference disc GPS Data. *J. Geod. Geodyn.* **2012**, *32*, 101–104.
17. Wang, W.; Wang, J.X.; Gao, J.Q. Cycle Slip Detection of GPS Data. *Geomat. Inf. Sci. Wuhan Univ.* **2010**, *35*, 667–690.
18. Feng, W.; Zhao, Y.; Zhou, L.; Huang, D.; Hassan, A. Fast cycle slip determination for high-rate multi-GNSS RTK using modified geometry-free phase combination. *GPS Solut.* **2020**, *24*, 42. [CrossRef]
19. Wang, L.X.; Gan, Y.; Sui, L.F. INS-aided single-frequency cycle-slip detection for kinematic GNSS. *Geomat. Inf. Sci. Wuhan Univ.* **2019**, *44*, 364–370.
20. Ju, B.; Gu, D.; Chang, X.; Herring, T.; Duan, X.; Wang, Z. Enhanced cycle slip detection method for dual-frequency BeiDou GEO carrier phase observations. *GPS Solut.* **2017**, *21*, 1227–1238. [CrossRef]
21. Yang, Z.; Liu, X.; Guo, J.; Xia, Y.; Chang, X. An enhanced method for detecting and repairing the cycle slips of dual-frequency onboard GPS receivers of LEO satellites. *J. Sens.* **2020**, *17*, 1–17. [CrossRef]
22. Liu, C.; Tao, Y.; Xin, H.; Zhao, X.; Zhou, T. A single-difference multipath hemispherical map for multipath mitigation in BDS-2/BDS-3 short baseline positioning. *Remote Sens.* **2021**, *13*, 304. [CrossRef]
23. Tao, Y.; Liu, C.; Liu, C.; Zhao, X.; Hu, H.; Xin, H. Joint time–frequency mask and convolutional neural network for real-time separation of multipath in GNSS deformation monitoring. *GPS Solut.* **2021**, *25*, 1–13. [CrossRef]